Improving surface-enhanced Raman scattering effect using gold-coated hierarchical polystyrene bead substrates modified with postgrowth microwave treatment

Clement Yuen
Wei Zheng
Zhiwei Huang
National University of Singapore
Bioimaging Laboratory
Department of Bioengineering
Faculty of Engineering
Singapore 117576

Abstract. We report a novel postgrowth microwave heating implementation by selectively modifying hierarchical polystyrene (PS) bead substrates coated with gold (Au) films to effectively improve the surface-enhanced Raman scattering (SERS) effect on the analytes. The SERS signal of probe molecule rhodamine 6G (Rh 6G) on the microwave-treated Au–PS substrates can be improved by 10-fold, while the detection limit of Rh 6G in concentration can be enhanced by two orders of magnitude compared to the as-growth substrates. The high-quality SERS spectrum of saliva can also be acquired using the modified substrates, demonstrating the potential for the realization of the high-performance SERS substrates for biomedical applications.
 [DOI: 10.1117/1.3050447]

Keywords: polystyrene bead; Raman spectroscopy; surface-enhanced Raman scattering; saliva.

Paper 08194R received Jun. 24, 2008; revised manuscript received Oct. 2, 2008; accepted for publication Nov. 5, 2008; published online Dec. 23, 2008.

1 Introduction

Raman spectroscopy is a vibrational spectroscopic technique that provides a wealth of information on molecular structures and conformations, surface processes, and interface reactions for chemical and biological analysis.[1–3] Despite all its advantages, the Raman intensity is inherently weak, preventing the possibility of achieving a low detection limit using conventional Raman spectroscopy.[2] In contrast, the surface-enhanced Raman scattering (SERS) effect[4,5] is able to enhance the Raman scattering cross section of molecules on the order of 10^6–10^{15} through the electromagnetic and chemical enhancements between metal nanostructures and target molecules in close proximity.[6,7] This makes the SERS technique an extremely sensitive biomolecular probe for single-molecule detection.[5,7] Recently, different types of SERS-active substrates, such as metal electrodes, colloidal aggregates, metal-coated nanostructures, and porous films,[8–10] have been developed to improve the SERS performance on analytes. Among the different SERS substrates, metal films coated on polystyrene (PS) nanospheres arrays have been demonstrated to be able to provide reproducible and predictable Raman enhancements in trace element analysis and also in high-throughput biosensing.[5,6] By varying the size of PS nanospheres and the thickness of the deposited gold (Au) films, the optimal excitation wavelengths can be tuned to the near-infrared (NIR) range that gives rises to the most favorable SERS performance of the substrates.[8,11] In addition, modifying the surface topography (in nanoscales) of the SERS substrates can also play an important role in influencing the SERS effect.[10–13] It was found that by fine-tuning the gap size of trenches and pores in Au film, surface roughness and nanostructures of surface topographic properties of the Au film in the substrates could be as critical as optimizing the geometries of the SERS substrates (e.g., thickness of the Au film and diameter of PS nanospheres) for improving the SERS effect.[10–13] Conventional heating methods (e.g., annealing samples in a heating oven[14]) may be used to modify the surface topography of the Au–PS substrates, but the high elevated temperature of all the substrates can result in the disfiguration of PS beads[15] prior to the effective modification of Au films, and thus, the SERS performance will be severely deteriorated.

In this work, we report a novel postgrowth microwave heating implementation by selectively modifying the Au surface topography of the Au-coated PS nanosphere arrays to establish SERS-active nanostructures for effectively improving the SERS performance. We characterize the surface topographic properties (e.g., surface morphologies and nanostructures) of microwave-treated Au–PS substrates. The selective heating ability of applying microwave technique on the Au–PS substrates and the influence of surface topographic variations on SERS effects, as well as the enhancement factor of the microwave-treated substrates are also investigated using the energy conservation and diffusion models.[16–18] We have also evaluated the SERS performance of the microwave-treated Au–PS substrates on probe molecule rhodamine 6G (Rh 6G) and bioanalyte-saliva.

Address all correspondence to: Zhiwei Huang, National University of Singapore, Bioimaging Laboratory, Department of Bioengineering, Faculty of Engineering, 9, Engineering Drive 1, Singapore 117576 E-mail: biehzw@nus.edu.sg

1083-3668/2008/13(6)/064040/7/$25.00 © 2008 SPIE

2 Materials and Methods

2.1 *Preparation of Au-Coated PS Beads with Postgrowth Microwave Heating*

We fabricated orderly arranged PS nanospheres (mean diameters of 500 nm, PolyScience Inc.) on a glass slide by using the sedimentation technique.[19] The volume fraction of the PS aqueous solution was 0.5 wt %. A 15-nm thick Au film was coated onto the PS beads (JOEL, JFC-1600 Auto fine coater). Finally, we introduced microwave heating (600 W at 2.45 GHz) to treat the entire SERS substrates with different treatment times to modify the shape of PS and Au nanostructures for improving SERS performance.

2.2 *Preparation of Analytes for SERS Experiments*

For SERS experiments on probe molecule Rh 6G, SERS substrates were dipped into aqueous solution of Rh 6G with concentrations ranging from 10^{-5} to 10^{-8} M under continue stirring for 10 min, rinsed with deionized water, and then dried up with nitrogen gas.[20] For evaluation of the SERS performance of modified substrates on saliva as a bioanalyte, the saliva samples were collected from 10 healthy volunteers 3 h after a meal and after 30 min of mouth rinsing. Particulates and exfoliated cells were separated from the saliva samples centrifuged at 14,000 rpm for 5 min (Sigma, Laborzentrifugen, 3K15). The upper layer of the centrifuged saliva samples was collected and deposited on the modified PS substrates for SERS measurements.

2.3 *Atomic Force Microscope (AFM)*

We employed AFM (Nanoscope IIIa, Digital Instruments) to quantitatively investigate the dimensions of nanostructures and surface roughness of the Au morphology on the PS beads.

2.4 *Scanning Electron Microscope (SEM)*

A SEM (JEOL, JSM-6700F) was used to examine the freestanding nanostructures and the surface morphology of the Au–PS bead substrate, with an accelerating voltage in the range of 10–15 kV.

2.5 *Raman Instrumentation*

We evaluated the SERS performance of the modified Au–PS bead substrates on the analytes (e.g., probe molecule Rh 6G, saliva) using a micro-Raman spectrometer system (inVia, Renishaw, UK) coupled with a microscope (DMI 5000M, Leica) in a backscattering geometry (Fig. 1). A Czerny-Turner–type spectrograph (f=250 mm) equipped with a holographic grating (1800 gr/mm) and an NIR-enhanced CCD detector (Peltier cooled at −70°C, Renishaw) were used for SERS spectrum measurements (spectral resolution of 2 cm^{-1}). A 785-nm laser beam (maximum output of 300 mW, Renishaw, UK) was focused onto the samples on the substrates with a power of 2.5 mW and a spot size of ~1 μm through an ultralong working distance water immersion microscope objective (63×, N.A. 0.9, Leica). Each SERS spectrum was collected with a signal integration time of 10 s, and averaged spectra were obtained from more than 10 different samples with a standard deviation of <5% for Rh 6G, and of <10% for saliva. Note that a third-order polynomial[3] was found to be optimal for fitting the broad fluorescence background in the raw spectrum; this polynomial was then subtracted from the raw spectrum to yield the SERS spectrum.

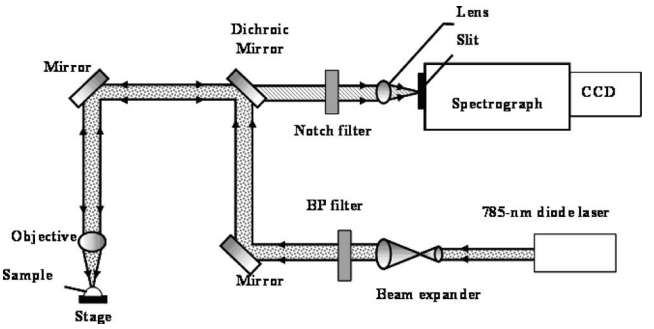

Fig. 1 Schematic of the Raman microscope system for SERS spectrum measurements.

3 Results

Figure 2(a) shows the SEM image of the Au–PS bead substrate treated with microwave heating time (T_{MW}) for 200 s (600 W at 2.45 GHz). Wirelike nanostructures are generated in the modified substrate [inset of Fig. 2(a)], leading to more effective SERS activities via the localization of electromagnetic waves on the sharp structures.[21] The wirelike nanostructures are probably formed from the discharge of Au film.[22] Au can be vaporized from the surface and condensed to form wirelike structures. In addition, the space between PS beads is reduced and the shape of PS is changed into a polyhedral shape, resulting in the changed spectral properties of the orderly PS structures. Although the shape of PS beads is modified, the hierarchical structure is preserved on the modified substrate to facilitate the redistribution of photon density of states and thus, promoting the optical modes density and Raman signals on analytes.[23]

Figure 2(b) gives the enlarged SEM image of Fig. 2(a), revealing the occurrence of Au ligaments and pores, as a consequence of the fusing of Au grains, and the Au film relaxation with the release of stress and the strain builtup during

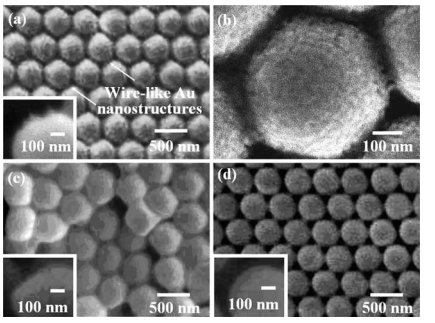

Fig. 2 (a) SEM image of Au films coated on the PS bead substrate (600 W, at 2.45 GHz, T_{MW}=200 s). (b) Locally enlarged SEM image of (a). SEM images of Au films coated on PS bead substrates (c) with hot plate heating (200°C for 200 s) and (d) without any postgrowth heat treatment. Inset in (a) highlights wirelike Au nanostructures on PS beads. Insets in (c) and (d) give the enlarged views of PS beads on the substrates with hot plate heating and without any heat treatment, respectively.

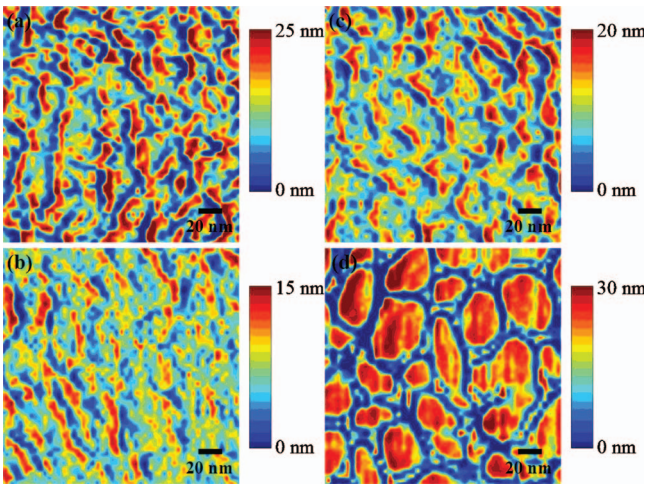

Fig. 3 AFM images of Au morphology on PS beads for each SERS substrate with different microwave heating times T_{MW} (600 W at 2.45 GHz): (a) 0, (b) 200, (c) 300, and (d) 600 s, respectively. Pseudo-color bars stand for the height of surface topography of the Au film on the PS bead substrate. AFM operating conditions (scan rate: 1.2 Hz; scan size: 0.2 nm; number of samples: 256).

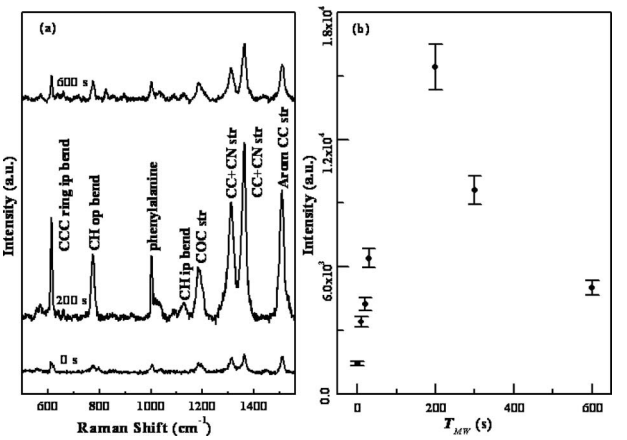

Fig. 4 (a) SERS spectra of Rh 6G (1×10^{-5} M) adsorbed on the Au–PS bead substrates with microwave treatment times T_{MW} (600 W, at 2.45 GHz) at 0, 200, and 600 s, respectively. (b) Dependence of SERS intensity at 1365 cm^{-1} (C–C/C–N stretching) of Rh 6G on Au–PS bead substrates with different microwave heating times T_{MW} (ip: in plane, bend: bending, op: out of plane, str: stretching, arom: aromatic).

the sputtering process. The nanometer gaps between the Au ligaments, known as a hot spot, give rise to intense electromagnetic fields.[9] In contrast, with the hot plate heating (200 °C for 200 s) as shown in Fig. 2(c), the periodic structures of substrates are disturbed, and the PS bead structure is deformed [highlighted in the inset of Fig. 2(c)]. Some PS beads are fused together indicating the inefficiency of selective heating by hot plates. Additionally, no wirelike nanostructures are formed in the hot plate–heated substrates because the arching of metal is inefficient. This indicates that employing conventional heating source to anneal Au–PS bead substrates is not effective in modifying the morphologies of metals, because high annealing temperature leads to the severe deformation of PS beads. For comparison purposes, Fig 2(d) shows the SEM image of Au–PS substrates without any treatment. The Au-coated PS beads are spherical in shape, and no wirelike nanostructures are observed [inset of Fig. 2(d)].

Figure 3 shows the AFM height images of the Au morphologies coated on PS beads from each microwave-treated substrate (600 W, at 2.45 GHz) with different T_{MW}. For the Au morphology on the PS beads of an as-growth substrate [Fig. 3(a), $T_{MW}=0$ s], the trenches and pores of Au ligaments have a mean value for the width or diameter, d, of ~13 nm, and a mean surface roughness, r, of ~12.26 nm. When T_{MW} is 200 s [Fig. 3(b)], the Au ligaments relax under microwave heating; thus, the value of d reduces to a minimum of ~8 nm, while the r value reduces to ~10.54 nm. When further increasing the microwave treating time ($T_{MW}>200$ s), Au grains and ligaments coalesce. For instance, in Fig. 3(c) ($T_{MW}=300$ s), the value of d is ~10 nm and r is ~13.83 nm. In Fig. 3(d) ($T_{MW}=600$ s), the value of d changes to ~15 nm and r increases to ~21.36 nm. Further SERS experiments in the following (Figs. 4 and 5) confirm the improvements of SERS signals to be related to the effective modifications of gap size and surface roughness of the Au film in the microwave-treated PS substrates.[5,24,25]

Figure 4(a) illustrates the SERS spectra of Rh 6G aqueous solution (1×10^{-5} M) adsorbed on the Au–PS bead substrates with different T_{MW}. Prominent Raman peaks, such as 615 cm^{-1} (C–C–C ring in-plane bending), 775 cm^{-1} (CH out-of-plane bending), 1130 cm^{-1} (CH in-plane bending), 1185 cm^{-1} (C–O–C stretching, phenylalanine), 1310 cm^{-1} (C–C/C–N stretching), 1365 cm^{-1} (C–C/C–N stretching), and 1508 cm^{-1} (aromatic C–C stretching),[26] respectively, are clearly discerned in probe molecule Rh 6G deposited on the microwave-treated substrates ($T_{MW}=200$ and 600 s). Figure 4(b) shows the dependence of Raman peak intensity at 1365 cm^{-1} on microwave heating times T_{MW}. We observe that a maximum SERS signal of Rh 6G occurs on the modified substrate with T_{MW} of ~200 s, which is approximately tenfold improvement compared to the as-growth substrate. The improvement of SERS performance of microwave-treated substrates could be mainly accounted by the collective influ-

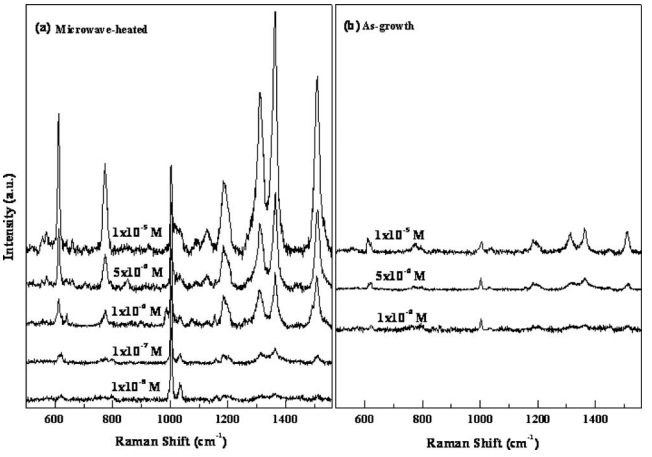

Fig. 5 SERS spectra of Rh 6G at different concentrations adsorbed on Au–PS bead substrates: (a) with microwave heating time of 200 s (600 W, at 2.45 GHz), and (b) without any heat treatment.

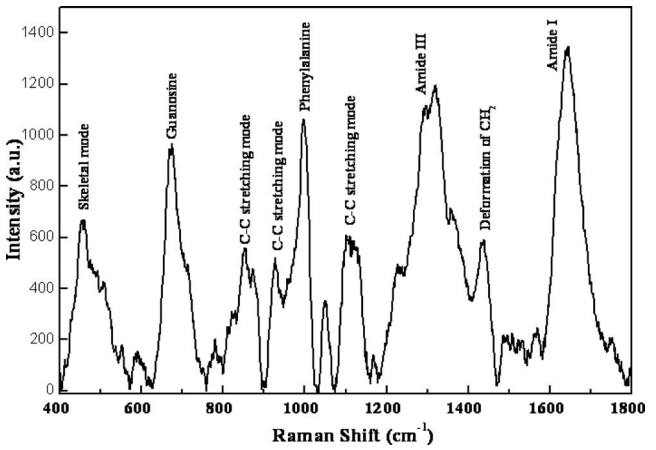

Fig. 6 SERS spectrum of saliva on Au films coated on the orderly PS bead substrate with postgrowth microwave heating (600 W, at 2.45 GHz, T_{MW}=200 s). The excitation power and the beam size of the 785-nm diode laser on the samples are 2.5 mW and ~1 μm, respectively. The integration time is 10 s for SERS spectrum acquisition. The broad background is subtracted from the raw SERS spectrum using a third-order polynomial fitting.[3]

ences from the modified Au morphologies, such as surface roughness,[5] gap size,[24,25] and the presence of wirelike nanostructures on the substrates.[21]

Figure 5 shows the comparison of SERS spectra of Rh 6G with different concentrations (varying from 10^{-5} to 10^{-8} M) adsorbed on: (a) microwave-treated substrates (T_{MW}=200 s) and (b) as-growth substrates. SERS spectra of Rh 6G with high signal-to-noise (S/N) ratios (10–30 for Rh 6G in concentrations of 10^{-8}–10^{-5} M) can be acquired using microwave-treated substrates. With the S/N ratio of 10 in Rh 6G SERS spectra acquired, the lowest detectable concentrations of Rh 6G for microwave-treated and as-growth substrates are 1×10^{-8} and 1×10^{-6} M, respectively. The above results confirm that microwave-treated substrates can lower the detection limit of Rh 6G by approximately two orders of magnitude in concentration compared to the as-growth substrates.

We also demonstrate the ability of the modified Au–PS bead substrate for improving SERS performance on bioanalytes. Figure 6 shows an example of SERS spectrum of saliva on the microwave-treated Au–PS substrate (600 W at 2.45 GHz for 200 s). Prominent vibrational features of saliva, including guanosine of nucleic acids at 668 cm^{-1}, phenylalanine band at 1004 cm^{-1}, amide III of proteins at 1305 cm^{-1}, CH_2 bending of proteins and lipids at 1440 cm^{-1}, and amide I of lysozyme proteins at 1645 cm^{-1}, can be distinguished in SERS spectra. Other weaker vibrational modes, such as phosphate at 450 cm^{-1}, C–C stretching of proteins and lipids at 853, 920, and 1125 cm^{-1}, respectively, are also clearly observed in saliva. The SERS peak positions of saliva are similar to conventional Raman studies on other biological tissues reported in the literature.[3,27–29] Hence, the high-quality SERS spectrum of saliva can be rapidly acquired using the modified Au–PS substrates.

4 Discussion

This study demonstrates that microwave heating method has the advantages of: (*i*) forming wirelike Au nanostructures, (*ii*) selectively modifying the Au sizes of ligaments and pores, and (*iii*) minimizing the thermal effect on Au–PS bead substrates, thereby leading to the much improved SERS-active structures of the Au–PS bead substrates. The possible mechanisms of the enhanced SERS effects of the microwave treated Au–PS bead substrates could be explained using the energy conservation and diffusion models[16,17] in the following.

We evaluate the fraction of the incident power absorbed (A) and the temperature change (ΔTemp) in the Au film and the PS beads layer of the SERS substrates during microwave heating treatment. With an approximation of the Au–PS bead substrate to be an Au film coated on the PS layer, the absorbed power (A) within the Au or PS layer can be determined using the energy conservation law,[16] $A=1-|R|^2-|T|^2*\mathrm{Re}[k_3/k_1]$, where R and T are the reflection and transmission coefficients, respectively. $k_1=\varpi\sqrt{\varepsilon_1\mu_1}$ and $k_3=\varpi\sqrt{\varepsilon_3\mu_1}$ are the wave numbers of the media for microwave propagation, whereby μ and ε stand for permeability and permittivity of the media, respectively.[30–32] Figure 7(a) shows the fractions of the incident power absorbed (A) within the Au film and the PS layer of the microwave-treated substrates (600 W at 2.45 GHz, T_{MW}=200 s). There is a maximum fraction (of ~38%) of the incident power deposited just beneath the surface (~0.3 nm) of the Au film, and then the deposited power quickly reduces to the level of 3% of the incident power at ~15 nm of the Au film. Because of the lower conductivity and higher permittivity in the PS film than in the Au film,[30–32] the fraction of the incident power deposition inside the PS beads layer is only in the range of $\sim3\times10^{-5}$%, which is almost six orders of magnitude less than that in the Au film. Hence, the incident microwave power is mostly absorbed by the Au film in the Au–PS bead substrate under microwave heating. With the selective microwave power absorption by the Au–PS bead substrate [Fig. 7(a)], the resulting temperature increase (ΔTemp) in the Au film and the PS layer can be estimated using the diffusion theory[17]

$$\Delta\mathrm{Temp}=100\frac{AS_{(x,y)}}{4\pi\kappa}\int_{-y/2}^{y/2}\int_{-x/2}^{x/2}1/(x^2+y^2)^{1/2}dxdy,$$

where κ is the thermal conductivity of the Au or PS film;[33–35] $S_{(x,y)}$ is an average Poynting flux of the incident power deposited onto the size $\Delta(x,y)$ of the SERS substrate;[35–39] A is the absorbed power in the microwave-treated Au–PS bead substrate [Fig. 7(a)]. Figure 7(b) illustrates the temperature change (ΔTemp) in the Au film and PS layer of the SERS substrate under microwave heating treatment (600 W at 2.45 GHz, T_{MW}=200 s). A sharp temperature increase, ΔTemp of ~1800 K, is found at the subsurface (~0.3 nm) of the Au film, and then the temperature change rapidly decays to ~150 K at ~15 nm. In contrast, the ΔTemp in the PS layer remains almost unchanged (<10 K), which is approximately 180-fold cooler than the temperature in the Au film. This indicates that the Au film can be efficiently heated up to a much greater extent than the PS bead layer by the microwave heating technique. For comparison purposes, we also investigate the temperature change of the Au film and the PS layer of the substrates under the hot plate heating treatment [200°C in Fig. 2(c)]. Assuming that the heat transfer in the Au–PS bead substrates under the hot plate heating treat-

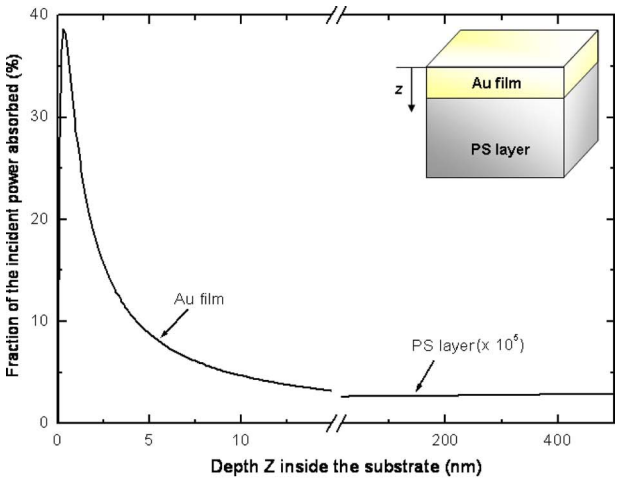

(a)

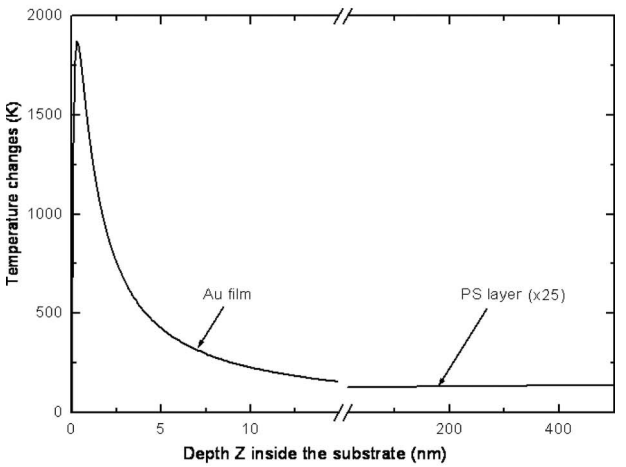

(b)

Fig. 7 (a) Comparison of fractions of the absorbed incident power (A) in the Au film and the PS beads layer of the substrates under microwave heating treatment (600 W at 2.54 GHz). Note that the absorbed power by the PS layer is magnified by 10^5 times for better display. The parameters used for calculation of the absorbed incident power (A) are adopted from Refs. 30–32. (b) Comparison of the temperature increase (ΔTemp) within the Au film and the PS beads layer of the substrates under microwave heating treatment (600 W at 2.54 GHz). Note that the temperature change in the PS layer is magnified by 25 times for better display. The parameters used for calculation of the temperature change are adopted from Refs. 37–39.

ment follows a steady-state heat conduction and convention in one dimension,[18] the temperature distributions within the Au film and the PS layer of the substrates are similar (<1 K in difference),[18,30,31] and approximately equal to the hot plate heating temperature of ~200°C (472 K) (detailed calculations not shown).

The above computation results confirm that the microwave heating technique can be very effective for modifying the Au morphologies of the Au–PS substrates, because the Au grains have more thermal energy (at least ~1800 K higher) for coalescence and relaxation of the Au films. With greater ease of coalescence and relaxation, the modifications of d and r can be facilitated, which is crucial to generating stronger SERS scattering (Fig. 3).[5,24,25] In addition, the temperature in the Au films is significantly higher (~1800 K higher) than the PS beads using the microwave heating technique, and thus, the minimized thermal effect in the PS layer enables an effective preservation of the orderly arranged structures of PS beads of the microwave-treated substrates [Fig. 2(a)] for improving SERS performance. Conversely, with the hot plate heating treatment on the Au–PS substrates, the temperature distribution between the Au film and the PS layer is almost the same (only ~0.01 K in difference), and thus, the relatively high-temperature increase (~472 K) in the PS layer severely disturbs the orderly arrangements of the PS beads [Fig. 2(c)], impairing the SERS performance of the Au–PS bead substrates. Therefore, the Au film absorbs more microwave power than the PS beads under the microwave heating process. The microwave heating technique can be used to selectively modify the surface topography (e.g., gap size, surface roughness, and wirelike structures) of the Au films, while preserving the hierarchical arrangements of PS beads of the substrates for effectively enhancing the SERS performance.

We also investigate the influence of surface topographic variations on the SERS performance of the Au–PS bead substrates under different treatment times of microwave heating. For substrates treated with $T_{MW} \leqq \sim 200$ s, the average gap size (d) for the trenches and pores of Au ligaments and the mean surface roughness (r) decrease with the increased treatment time. d ~8 nm and r ~10.54 nm are at minimum for substrates with $T_{MW} = \sim 200$ s [Fig. 3(b)]. The reduced gap size (d) of the Au film of the substrates can improve the local electric field (E_{local}), because E_{local} is proportional to $1/d^3$.[36] As such, the electromagnetic field enhancement in SERS, which is proportional to $|E_{local}|^4$, can be greatly enhanced by reducing d.[36] Although the reduction in surface roughness (r) from ~12.26 nm [Fig. 3(a)] to ~10.54 nm [Fig. 3(b)] during the increased microwave heating times (T_{MW}=0–200 s) may weaken the SERS effect due to the impediment in the radiation of surface plasmon energy,[37,38] a tenfold improvement in SERS intensity is still observed in our substrates with $T_{MW} = \sim 200$ s (Fig. 4). This observation indicates that the gap-size effect and wirelike nanostructures are the more dominant enhancement factor in SERS effect when $T_{MW} \leqq 200$ s. When $T_{MW} > 200$ s [Figs. 3(c) and 3(d)], the values of d and r increase in the microwave modified substrates. For instance, when T_{MW} increases to ~600 s, d increases from ~13 nm [Fig. 3(a)] to ~15 nm [Fig. 3(d)] and r increases from ~12.26 nm [Fig. 3(a)] to ~21.36 nm [Fig. 3(d)]. Despite that the increment of d could lead to a weaker SERS effect, the Raman intensity observed is still about three times higher than the as-growth substrate (Fig. 4). This suggests that the effect of surface roughness (r) can also play a dominant role in enhancing the SERS effect when $T_{MW} > 200$ s. Therefore, the improved SERS performance of our microwave-treated Au–PS bead substrates could be attributed to the combined result of various enhancement factors working together, such as gap-size variations, the surface roughness, and the localization of electromagnetic waves arising from wirelike nanostructures.[5,21,24,25]

To gain further insight into the exhibited enhancement behavior, we also estimate the enhancement factor (EF) of the microwave-treated substrates by measuring the SERS spectra of p-aminobenzoic acid (PABA) on the microwave-treated

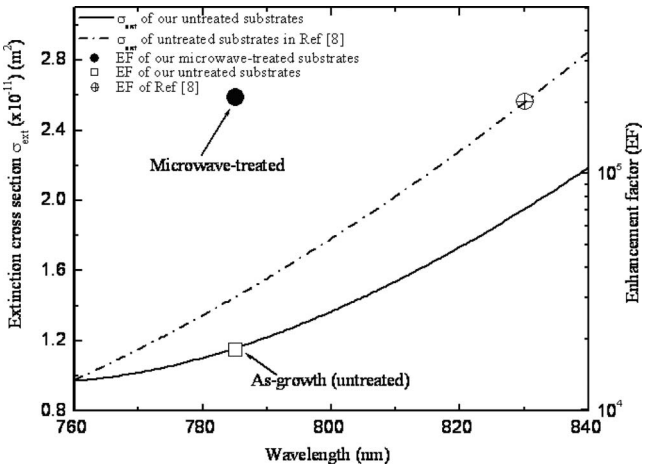

Fig. 8 EF of our substrates (500-nm PS bead core coated with 15-nm Au shells: microwave treated, ●; untreated, □) and the untreated substrates reported in Ref. 8 (400-nm PS bead core coated with 15-nm Au shells: ⊕). Comparison of the extinction cross section σ_{ext} of our untreated substrates (500-nm PS bead core coated with 15-nm Au shells) and the untreated substrates reported in Ref. 8 (400-nm PS bead core coated with 15-nm Au shells).

Au-coated PS bead substrates and the post-growth (untreated) Au-coated PS bead substrates (Fig. 8). We find that the EF of the microwave-treated substrates ($T_{MW}=200$ s) is approximately 1.8×10^5 using PABA under the 785-nm laser excitation (spectra not shown), which is about ten times higher than the as-growth (untreated) substrates. Again, the much improved EF of our microwave-treated substrates can be attributed to the enhancement factors related to the modifications of surface morphologies and substrate geometries under microwave heating treatment, as discussed above.[5,21,24,25] To compare the EF of our microwave-treated substrate to that of the untreated Au–PS bead substrates reported in Ref. 8, we calculate the extinction cross sections (σ_{ext}) of these substrates based on the scattering theory:[31] $\sigma_{ext}=k^4|\alpha|^2/(6\pi\varepsilon_o^2)+k\,\mathrm{Im}(\alpha)/\varepsilon_o$ (k is the wave vector of the incident wave, α is the polarizability, and ε_o is the permittivity of free space[31]). Figure 8 shows the comparison of the extinction cross sections σ_{ext} of our untreated substrates and the substrate reported in Ref. 8 at different wavelengths. Although the maximum σ_{ext} of our untreated Au–PS substrates (500-nm PS bead core with 15-nm Au shell) is slightly shifted to a longer wavelength compared to the reported substrates (400-nm PS bead core with 15-nm Au shell),[8] our microwave-treated Au–PS substrates ($T_{MW}=200$ s) still remain at a similar high EF (of $\sim1.8\times10^5$ at 785 nm) in comparison to the substrates (e.g., EF of $\sim1.23\times10^5$ at 830 nm).[8] This is probably due to the effective modifications of the Au surface morphologies of our microwave-treated Au–PS substrates, the modified Au-coated PS beads with smaller d and r values [Fig. 3(b)] can be analogous to the nanoparticles with a smoother surface that exhibits a much improved higher-order multipolar resonances.[39] As such, the extinction spectra of our microwave-treated substrates can be blueshifted to the shorter wavelengths,[39] causing σ_{ext} at 785 nm to increase with an improved EF (tenfold improvements in EF compared to the as-growth substrates) (Fig. 8). These results further demonstrate the efficacy of the microwave heating technique in selectively modifying the Au surface morphology to enhance the extinction cross sections of the Au–PS bead substrates, leading to a much improved SERS performance.

5 Conclusions

We first report the well-controlled postgrowth microwave treatment on the Au–PS bead substrates for effectively improving the SERS performance. This method enables the selective modification and discharging of Au films while minimizing the thermal effect on PS beads, thereby promoting greatly enhanced SERS activities. We find that using the modified Au–PS substrates, the SERS signals of Rh 6G can be improved tenfold, while the detection limit of Rh 6G in concentrations can be improved by two orders of magnitude compared to the as-growth substrates. Furthermore, high-quality SERS spectra of saliva can also be acquired using the modified substrates, demonstrating the great promise for the realization of high-performance SERS substrates for biomedical applications.

Acknowledgments

This research was supported by the Academic Research Fund from the Ministry of Education, the Biomedical Research Council, the National Medical Research Council, and the Faculty Research Fund from the National University of Singapore.

References

1. C. V. Raman and K. S. Krishnan, "A new type of secondary radiation," *Nature* **121**(4), 501–502 (1928).
2. R. M. Jarvis and R. Goodacre, "Characterization and identification of bacteria using SERS," *Chem. Soc. Rev.* **37**(5), 931–936 (2008).
3. Z. Huang, A. McWilliams, H. Lui, D. I. McLean, S. Lam, and H. Zeng, "Near-infrared Raman spectroscopy for optical diagnosis of lung cancer," *Int. J. Cancer* **107**(6), 1047–1052 (2003).
4. M. Fleischmann, P. J. Hendra, and A. J. McQuillan, "Raman spectra of pyridine adsorbed at a silver electrode," *Chem. Phys. Lett.* **26**(2), 163–166 (1974).
5. J. N. Anker, W. P. Hall, O. Lyandres, N. C. Shah, J. Zhao, and R. P. Van Duyne, "Biosensing with plasmonic nanosensors," *Nature Mater.* **7**(6), 442–453 (2008).
6. S. E. J. Bell and N. M. S. Sirimuthu, "Quantitative surface-enhanced Raman spectroscopy," *Chem. Soc. Rev.* **37**(5), 1012–1024 (2008).
7. N. P. W. Pieczonka and R. F. Aroca, "Single molecule analysis by surfaced-enhanced Raman scattering," *Chem. Soc. Rev.* **37**(5), 946–954 (2008).
8. L. Baia, M. Baia, J. Popp, and S. Astilean, "Gold films deposited over regular arrays of polystyrene nanospheres as highly effective SERS substrates from visible to NIR," *J. Phys. Chem. B* **110**(47), 23982–23986 (2006).
9. L. H. Qian, X. Q. Yan, T. Fujita, A. Inoue, and M. W. Chen, "Surface enhanced Raman scattering of nanoporous gold: Smaller pore sizes stronger enhancements," *Appl. Phys. Lett.* **90**(15), 153120 (2007).
10. M. E. Stewart, C. R. Anderton, L. B. Thompson, J. Maria, S. K. Gray, J. A. Rogers, and R. G. Nuzzo, "Nanostructured plasmonic sensors," *Chem. Rev. (Washington, D.C.)* **108**(2), 494–521 (2008).
11. S. Lal, N. K. Grady, J. Kundu, C. S. Levin, J. B. Lassiter, and N. J. Halas, "Tailoring plasmonic substrates for surface enhanced spectroscopies," *ScienceAsia* **37**(5), 898–911 (2008).
12. C. Yuen, W. Zheng, and Z. Huang, "Surface-enhanced Raman scattering: principles, nanostructures, fabrications and biomedical applications," *J. Innovative Opt. Health Sci.* **1**(2), 267–284 (2008).
13. J. Biener, G. W. Nyce, A. M. Hodge, M. M. Biener, A. V. Hamza, and S. A. Maier, "Nanoporous plasmonic matamaterials," *Adv. Mater. (Weinheim, Ger.)* **20**(6), 1211–1217 (2008).
14. E. Piscopiello, L. Tapfer, M. V. Antisari, P. Paiano, P. Prete, and N.

Lovergine, "Formation of epitaxial gold nanoisland on (100) silicon," *Phys. Rev. B* **78**(3), 035305 (2008).
15. B. Gates, S. H. Park, and Y. Xia, "Tuning the photonic bandgap properties of crystalline arrays of polystyrene bends by annealing at elevated temperatures," *Adv. Mater. (Weinheim, Ger.)* **12**, 653–656 (2000).
16. D. Razansky, P. D. Einziger, and D. R. Adam, "Broadband absorption spectroscopy via excitation of lossy resonance modes in thin films," *Phys. Rev. Lett.* **95**(1), 018101 (2005).
17. H. Bosman, Y. Y. Lau, and R. M. Gilgenbach, "Microwave absorption on a thin film," *Appl. Phys. Lett.* **82**(9), 1353–1355 (2003).
18. D. R. Pitts and L. E. Sissom, *Schaum's Outline of Theory and Problems of Heat Transfer*, McGraw-Hill, New York (1998).
19. N. D. Denkov, O. D. Velev, P. A. Kralchevsky, I. B. Ivanov, H. Yoshimura, and K. Nagayama, "Mechanism of formation of two-dimensional crystals from latex particles on substrates," *Langmuir* **8**(12), 3183–3190 (1992).
20. A. Nakajima, N. Horimoto, and N. Ishikawa, "Preparation of a SERS substrate using vacuum-synthesized silver nanoparticles," *Chem. Phys. Lett.* **413**(1–3), 78–83 (2005).
21. E. Bailo and V. Deckert, "Tip-enhanced Raman scattering," *Chem. Soc. Rev.* **37**(5), 921–930 (2008).
22. D. F. Farson, H. W. Choi, and S. I. Rokhlin, "Electrical discharges between platinum nanoprobe tips and gold films at nanometer gap lengths," *Nanotechnology* **17**(1), 132–139 (2006).
23. S. V. Gaponenko, "Effects of photon density of states on Raman scattering in mesoscopic structures," *Phys. Rev. B* **65**(14), 140303 (2002).
24. I. Pavel, E. McCarney, A. Elkhaled, A. Morrill, K. Plaxco, and M. Moskovits, "Label-free SERS detection of small proteins modified to act as bifunctional linkers," *J. Phys. Chem. C* **112**(13), 4880–4883 (2008).
25. S. A. Maier, "Plasmonic field enhancement and SERS in the effective mode volume picture," *Opt. Express* **14**(5), 1957–1964 (2006).
26. M. Baia, L. Baia, and S. Astilean, "Gold nanostructured films deposited on polystyrene colloidal templates for surface-enhanced Raman spectroscopy," *Chem. Phys. Lett.* **404**(1–3), 3–8 (2005).
27. Y. Nishimura, M. Tsuboi, and T. Sato, "Structure-spectrum correlations in nucleic acids. I. Raman lines in the 600–700 cm^{-1} range of guanosine residue," *Nucleic Acids Res.* **12**(17), 6901–6908 (1984).
28. S. K. Teh, W. Zheng, K. Y. Ho, M. Teh, K. G. Yeoh, and Z. Huang, "Diagnostic potential of near-infrared Raman spectroscopy in the stomach: Differentiating dysplasia from normal tissue," *Br. J. Cancer* **98**(2), 457–465 (2008).
29. Z. Huang, H. Lui, D. McLean, M. Korbelik, and H. Zeng (2005), "Raman Spectroscopy in combination with background near-infrared autofluorescence enhances the *in vivo* assessment of malignant tissues," *Photochem. Photobiol.* **81**(5), 1219–1226 (2005).
30. C. F. Coombs, *Printed Circuit Handbook*, McGraw-Hill, New York (2001).
31. R. D. Averitt, S. L. Westcott, and N. J. Halas, "Linear optical properties of gold nanoshells," *J. Opt. Soc. Am. B* **16**(10), 1824–1832 (1999).
32. G. Chen, P. Hui, K. Pita, P. Hing, and L. Kong, "Conductivity drop crystallites redistribution in gold film," *Appl. Phys. A* **80**(3), 659–665 (2005).
33. B. I. Kilkis and A. S. R. Suntur, "Development of a unified heat transfer model with special emphasis on thermal conduction," *Int. Commun. Heat Mass Transfer* **26**(5), 657–667 (1999).
34. R. B. Stephens, G. S. Cieloszyk, and G. L. Salinger, "Thermal conductivity and specific heat of non-crystalline solids:polystyrene and polymethyl methacrylate," *Phys. Lett. A* **38**(3), 215–215 (1972).
35. H. Ni, A. K. Datta, and R. Parmeswar, "Moisture loss as related to heating uniformity in microwave processing of solid foods," *J. Food Process Eng.* **22**(5), 367–382 (1999).
36. S. A. Maier, M. L. Brongersma, P. G. Kik, and H. A. Atwater, "Observation of near-field coupling in metal nanoparticle chains using far-field polarization spectroscopy," *Phys. Rev. B* **65**(19), 193408 (2002).
37. M. Moskovits,"Surface-enhanced spectroscopy," *Rev. Mod. Phys.* **57**(3), 783–826 (1985).
38. A. G. Brolo, D. E. Irish, G. Szymanski, and J. Lipkowski, "Relationship between SERS intensity and both surface coverage and morphology for pyrazine adsorbed on a polycrystalline gold electrode," *Langmuir* **14**(2), 517–527 (1998).
39. H. Wang and N. J. Halas, "Mesoscopic Au 'meatball' particles," *Adv. Mater. (Weinheim, Ger.)* **20**(4), 820–825 (2008).